Phase-space computation of multi-arrival traveltimes: Part II – Implementation and application to angle-domain imaging

Vladimir Bashkardin[1], Thomas J. Browaeys[2], Sergey Fomel[1], Fuchun Gao[3], Scott A. Morton[4], Sergey Terentyev[4], and Alexander Vladimirsky[5]

SUMMARY

Computation of multi-arrival traveltimes for angle-domain Kirchhoff migration is most simply performed by ray tracing from subsurface points. However, the high computational cost of this approach limits its feasibility in practice. Fortunately this ray-tracing procedure can be replaced by the faster computation of escape variables in phase space. In this paper, we provide details of our implementation of an escape-equation solver and address the challenges of the scalability of this method in 3-D. We introduce the "narrow band" concept, which enables solution of large-scale 3-D problems. The resultant algorithm produces accurate traveltimes and provides input for angle-domain imaging.

INTRODUCTION

Kirchhoff migration has been the workhorse for iterative imaging and model building in the petroleum industry for the last thirty years. Formulated in its classic form as a surface integral (Schneider, 1978), it provides a straightforward way to generate target-oriented output and produce offset gathers. The standard Kirchhoff kernel uses single-valued traveltimes computed from surface locations to subsurface image points. It has been shown that, for complex geology and in the presence of traveltime multipathing, such a migration does not provide accurate enough images (Operto et al., 2000), and it is prone to kinematic and dynamic errors (Xu et al., 2001; Stolk and Symes, 2004).

A different approach to Kirchhoff migration is based on the generalized Radon transform (Beylkin, 1985), which introduces accurate weights related to reflectivity for true-amplitude migration (Miller et al., 1987). However, the original formulation for integration in the surface coordinate system does not take into account the possible development of multi-valued traveltimes and requires computation of the Beylkin determinant (Bleistein, 1987). Both obstacles can be removed if the integration is performed in subsurface angular coordinates over source and receiver branches. This unravels multipathing and establishes an imaging domain in which surface data are mapped to subsurface points as a function of scattering and dip angles (Xu et al., 2001; Brandsberg-Dahl et al., 2003; Sava and Fomel, 2003; Bleistein et al., 2005). Output angle gathers provide an ideal image representation for AVA (amplitude versus angle) analysis and, in theory, can be free of the kinematic and dynamic errors mentioned above.

Rays can be simply traced from image locations to the acquisition surface so as to compute multi-arrival traveltime tables for angle migration. Such a bottom-up approach enables one-to-one mapping between subsurface locations/subsurface slowness vector and exit locations (surface point)/exit ray parameter (Koren et al., 2002; Koren and Ravve, 2011), thus avoiding ambiguity between different ray branches when rays are shot from the surface (Xu and Lambaré, 2004). In practice, bottom-up ray tracing is usually done for sparse subsurface locations (Ettrich et al., 2008). Ray shooting on a dense grid for higher traveltime resolution appears computationally expensive. Alternatively, initial-value ray tracing can be reformulated in the form of escape equations (Fomel and Sethian, 2002; Bashkardin et al., 2012), which allow for a faster computation of angle-migration traveltime tables on a phase-space grid.

In this paper, we briefly recap the principles of the stable discretization of escape equations and explain our implementation of an accurate, scalable escape-equation solver. We introduce the narrow-band concept, which enables application of the solver to large-scale 3-D problems. We demonstrate that our algorithm produces accurate traveltimes for a 3-D subsalt environment and show how its output can be used directly by angle-domain migration.

KIRCHHOFF MIGRATION IN ANGLE DOMAIN

The conventional Kirchhoff imaging operator is

$$I(\mathbf{x}) = \iint W(\mathbf{x},\mathbf{s},\mathbf{r})\,\mathbf{D}_t u\left[\mathbf{s},\mathbf{r},T(\mathbf{s},\mathbf{x})+T(\mathbf{r},\mathbf{x})\right] d\mathbf{s}\,d\mathbf{r}\;, \quad (1)$$

where $\mathbf{x}$ is the subsurface (image) location, u is the wavefield recorded at the surface, $\mathbf{D}_t$ is the waveform correction operator, $\mathbf{s}$ and $\mathbf{r}$ are the shot and receiver positions on the surface, T is the traveltime from the surface to $\mathbf{x}$, and W is the amplitude weight. If multipathing occurs in the subsurface, then the two-point traveltime T may have more than one value. However, if the integral is rewritten in a subsurface coordinate system as (Xu et al., 2001)

$$I(\mathbf{x}) = \iint \widehat{W}(\mathbf{x},\mathbf{p}_s,\mathbf{p}_r)\,\mathbf{D}_t u\Big[\widehat{\mathbf{y}}(\mathbf{x},\mathbf{p}_s),\widehat{\mathbf{y}}(\mathbf{x},\mathbf{p}_r), \widehat{T}(\mathbf{x},\mathbf{p}_s)+\widehat{T}(\mathbf{x},\mathbf{p}_r)\Big]\, d\mathbf{p}_s\,d\mathbf{p}_r\;, \quad (2)$$

where $\mathbf{p}$ is the phase slowness vector for a ray originating from $\mathbf{x}$ and $\widehat{T}$ is the escape traveltime for it at the escape position $\widehat{\mathbf{y}}$ on the surface, then, unlike the surface-to-subsurface traveltime T in equation 1, its counterpart $\widehat{T}$ is uniquely parameterized by the subsurface vector $\mathbf{p}$ and is strictly single-valued (neglecting ray splitting at interfaces).

[1]The University of Texas at Austin
[2]The University of Texas at Austin (now at Total E&P)
[3]Total E&P
[4]Hess Corporation
[5]Cornell University

DOI http://dx.doi.org/10.1190/segam2012-1537.1

Ray tracing from all subsurface locations in all directions in the whole domain eventually generates a set of escape volumes, $\widehat{\mathbf{y}}$ and $\widehat{T}$, required by migration. These volumes can instead be computed with less computational cost with the help of escape equations (Fomel and Sethian, 2002).

In Part I (Bashkardin et al., 2012), We derived the escape equations for general anisotropic media and constructed their corresponding reduced-phase-space representations. Instead of calculating each ray trajectory individually, these equations compute a flow of an escape variable inside phase space by using a local numerical stencil. Computationally, this Eulerian approach is more efficient than Lagrangian tracing of separate rays.

IMPLEMENTATION OF ESCAPE-EQUATION SOLVER

Escape equations and discretization

For angle-domain imaging in 3-D, a minimum set of four escape volumes should be computed: escape coordinates $\widehat{x}$, $\widehat{y}$, $\widehat{z}$, and escape traveltime $\widehat{T}$. Computation of each escape volume uses its own set of boundary conditions and its own right-hand side. The coefficients in the escape equations depend only on the background slowness; hence the same numerical scheme is used for all escape volumes. Other escape quantities, such as the escape phase vector $\widehat{\mathbf{p}}$, if required by a particular migration implementation, can be computed with appropriate boundary conditions and appropriate right-hand sides.

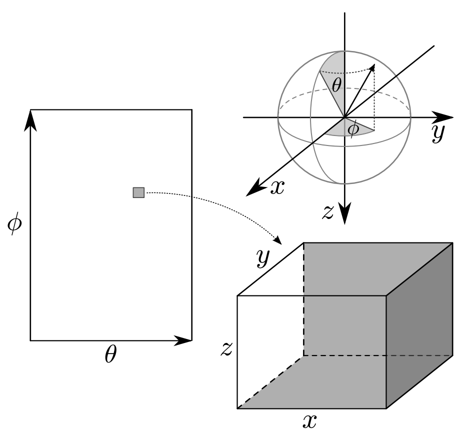

Figure 1: 5-D reduced phase space and boundary conditions for escape equations (θ - inclination, ϕ - azimuth angle)

In Part I (Bashkardin et al., 2012), we introduced upwind finite differences of the first and second order for a stable discretization of the escape equations. The order of the F-D stencil depends on the local gradient of the escape solution. After discretization, the escape equations turn into a sparse linear system, which we solve using Gauss-Seidel updates and alternating sweeping directions.

The upper part of Figure 2 displays boundary condition patches for a 2-D slowness model in 3-D reduced phase space. For a 3-D model, dimensionality of the reduced phase space increases to five (Figure 1); in other words, every location in 2-D angular grid contains a full 3-D x-y-z volume. Each of the volumes contains boundary condition points defined on its surface.

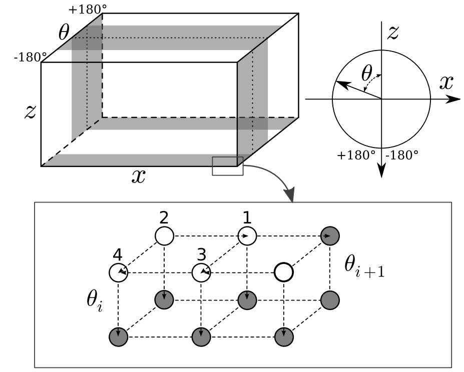

Figure 2: Boundary conditions for escape equations (shaded in grey) in 3-D reduced phase space (top); close-up of phase-space grid (bottom): gray points have known values, white points are to be computed, Point-1 and Point-2 belong to a different phase direction than do Point-3 and Point-4.

Spatial sampling of the phase-space grid should be close to the sampling of the slowness model. However, for a slowness model with considerable gradients this is not usually sufficient and leads to errors in the solution if only finite differences are used. As explained in Part I, we choose to avoid grid refinement in such cases and fix escape values in particularly difficult places using explicit ray tracing. For such a hybrid scheme, angular spacing of 1° appears to offer the optimal resolution for imaging.

Scalability and the narrow band

The approach described above enables the computations of a full escape solution for a 2-D general media. However, it keeps the full solution vector in computer memory, which turns out to be unfeasible for 3-D models and the corresponding 5-D reduced phase space. For a typical model and discretization (N_x=N_y $\approx$ 1000-1500 grid points, Δx=Δy=25 m, N_z $\approx$ 500-1200 points, Δz=12.5 m,$\Delta\theta = \Delta\phi = 1^\circ$) and four escape variables, a full solution vector would require between 500 and 3500 Tb of memory. We can alleviate this problem if we solve escape equations for smaller subdivisions of angular directions independently.

In 2-D, we can divide θ into two parts: upgoing $\theta = (-90^\circ;+90^\circ)$ and downgoing $\theta = (-180^\circ;-90^\circ)$, $(+90^\circ;+180^\circ)$. This division, however, means that the θ direction is not periodic anymore. Therefore, for each new part of the phase-space grid, we have to introduce extra boundary conditions in θ, which we can compute using ray tracing. Given the above discretization, this computation is a minor overhead for the algorithm.

Moreover, we can observe that the solution in each of the subdivisions can be computed gradually along the z direction in a thin layer – the narrow band. This band stretches along the x direction and contains unknown points for the current z level and points with known values from h previous z levels (h is the order of the F-D stencil in use). At the beginning of the process, these known values (parent points) are provided by

DOI http://dx.doi.org/10.1190/segam2012-1537.1

boundary conditions on the x-θ plane. For the current z location of the band, the same iterative scheme with alternating directions is used to obtain values for unknown points. The narrow band then moves down to the next level, the uppermost layer of parent points in the band is removed, and the newly computed points become a layer of parents for unknown points at the new level.

In (N_z - 1) steps, a complete solution to the downgoing divion of the phase-space grid is obtained. The same process is repeated for the upgoing part in the opposite direction along z. The full solution for all phase directions is a combination of outputs of the two narrow-band progressions.

Similarly, in 3-D, the narrow band is divided into two parts, downgoing and upgoing, with borders provided by ray tracing. The size of the band in 3-D is

$$w = N_x N_y \frac{N_\theta}{2} N_\phi \; (h+1) \; .$$

Instead of storing the whole escape-solution vector in computer memory, this technique permits keeping only a small division and building a solution in steps. For the aforementioned phase-space size range of 500 to 3500 Tb, the corresponding narrow band occupies 1.5 to 3.5 Tb.

We parallelize this narrow-band solver by dividing the angular $\theta - \phi$ domain into smaller subdomains, which we distribute across the nodes of a computer cluster. These subdomains exchange boundary information after each sweeping iteration.

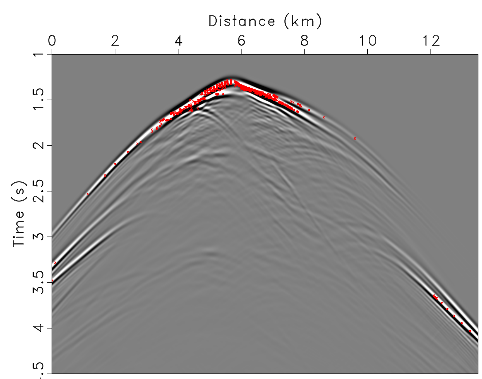

Figure 3: Escape traveltimes and positions marked on recorded wavefield at x=6.75 km for SEG/EAGE salt model and a source at (x, y, z) = (7,6,3) km.

RESULTS

Arrivals matching tests

We test the accuracy of the escape-equation solver in 3-D by matching arrivals of a simulated wavefield against the computed escape values for the same points in the subsurface. Figure 3 shows the wavefield recorded on the surface of the SEG/EAGE salt model for a source under the salt body. Extracted escape positions in the vicinity of this line and the same subsurface point are plotted in red and present a good match and coverage for the wavefront positions.

Angle-domain migration

We perform integration in equation 2 over the corresponding angular directions θ and ϕ and build opening- and dip-angle gathers. For 2-D migration, the opening angle is $\gamma = (\theta_s - \theta_r)$, and the dip angle is $\nu = (\theta_s + \theta_r)/2$. Because exit locations do not coincide with actual source and receiver positions, we look instead at pairs of neighbor phase directions so as to identify a local accumulation area on the surface for the two branches (Figure 4). Solution of the escape equations provides all the information necessary for this processl; $\widehat{z}(\mathbf{x}, \theta)$ is used to find the arrivals exiting on the surface, $\widehat{x}(\mathbf{x}, \theta)$ is used to build source/receiver branches, and $\widehat{T}(\mathbf{x}, \theta)$ pinpoints the time for each branch. Geometrical spreading required by the amplitude weight and KMAH index are determined from the escape solutions as well. Accumulated data points are properly weighted by hitcounts (Audebert et al., 2003).

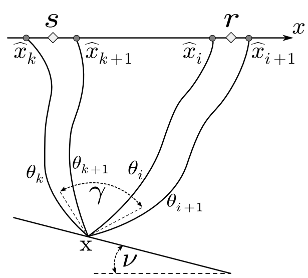

Figure 4: Construction of source and receiver branches from escape quantities for 2-D migration in angle domain.

Figure 6 shows the migration result of the Hess VTI model data with the above migration approach and escape solutions computed by our escape-equation solver. The low-amplitude reservoir target (right of the salt body, z=3-4 km) is correctly positioned and visible in the image and the gathers (Figure 7(b)).

Figure 5 presents the angle-domain image in the angle domain for the Sigsbee2b data. Migration with the escape solutions produces a continuous salt boundary and reveals most of the bottom target horizon in the subsalt area.

Conclusions

We have presented the implementation of an escape-equation solver with narrow-band support. It embodies an efficient hybrid Eulerian-Lagrangian algorithm and allows the calculation of escape solutions with accuracy that are sufficient for imaging in highly heterogeneous anisotropic media. We have demonstrated that output generated by this implementation can be used directly with angle-domain Kirchhoff migration. Because all of the geometrical information is embedded in escape solutions, they can be used for other tasks, such as angle-domain velocity estimation.

ACKNOWLEDGMENTS

We thank Hess and Total for supporting this work and permission to publish the results. We acknowledge the Texas Advanced Computing Center (TACC) at The University of Texas at Austin for providing HPC resources.

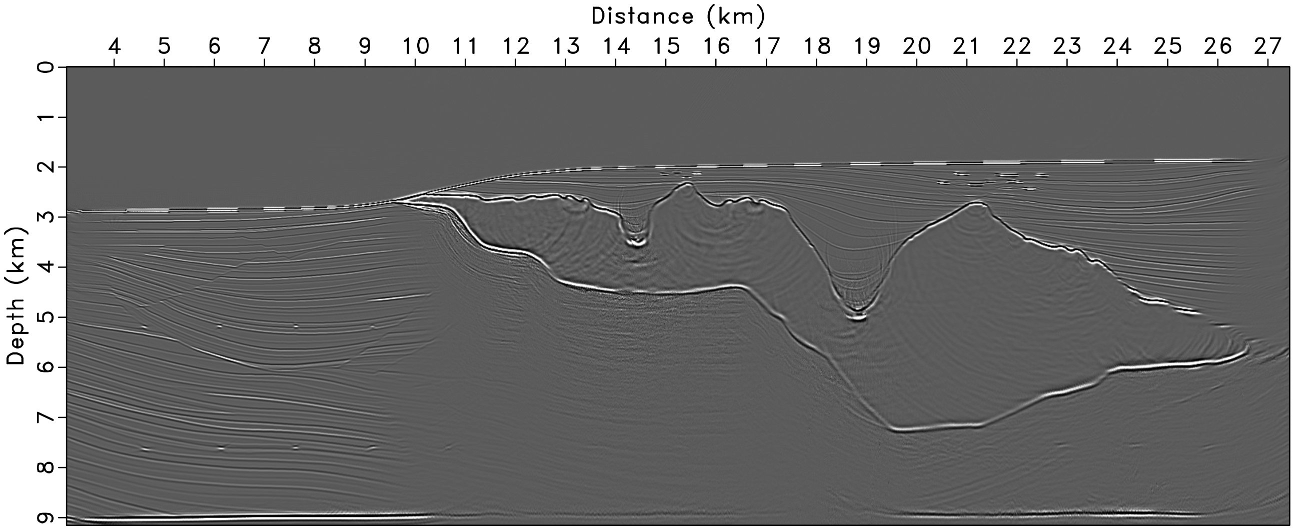

Figure 5: Angle-domain migration of Sigsbee2b model using phase-space traveltimes.

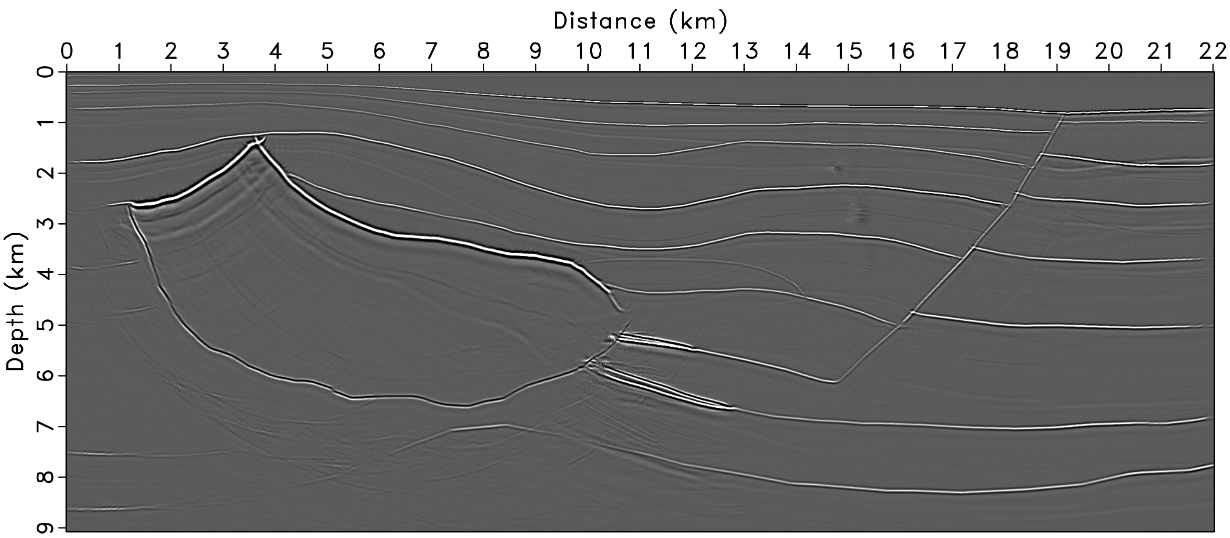

Figure 6: Angle-domain migration of Hess VTI model using phase-space traveltimes.

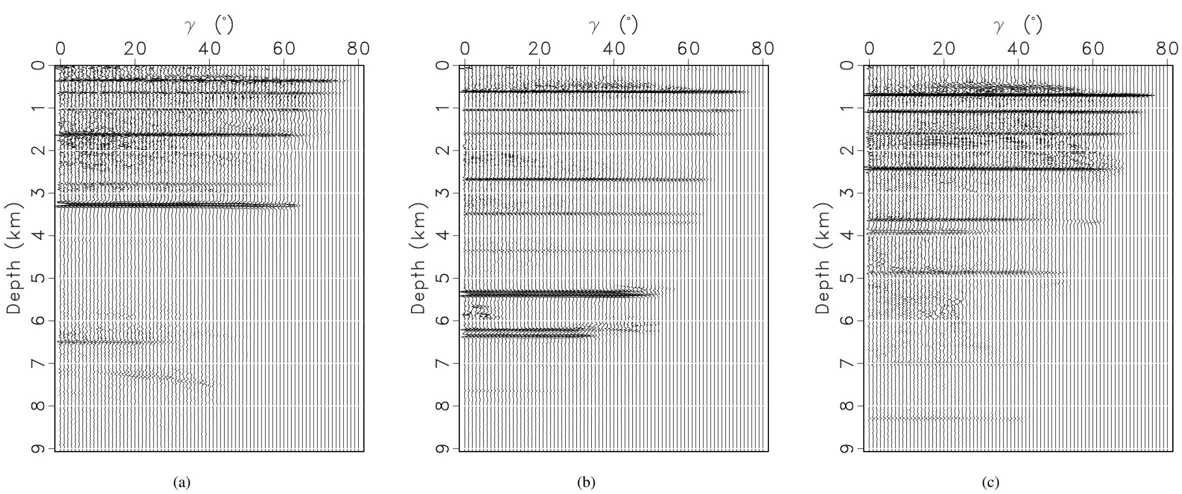

Figure 7: Opening angle gathers at 7 km (a), 11.5 km (b) and 17 km (c) for the Hess VTI image.

DOI http://dx.doi.org/10.1190/segam2012-1537.1

http://dx.doi.org/10.1190/segam2012-1537.1

EDITED REFERENCES

Note: This reference list is a copy-edited version of the reference list submitted by the author. Reference lists for the 2012 SEG Technical Program Expanded Abstracts have been copy edited so that references provided with the online metadata for each paper will achieve a high degree of linking to cited sources that appear on the Web.

REFERENCES

Audebert, F., L. Nicoletis, P. Froidevaux, and H. Rakotoarisoa, 2003, True amplitude migration in the angle domain by regularization of illumination: 73rd Annual International Meeting, SEG, Expanded Abstracts, 921–924.

Bashkardin, V., T. J. Browaeys, S. Fomel, F. Gao, R. Kazinnik, S. A. Morton, S. Terentyev, A. Vladimirsky, and P. Williamson, 2012, Phase-space computation of multi-arrival traveltimes: Part I — Theory and concepts: 82nd Annual International Meeting, SEG, Expanded Abstracts, submitted.

Beylkin, G., 1985, Imaging of discontinuities in the inverse scattering problem by inversion of a causal generalized Radon transform: Journal of Mathematical Physics, **26**, 99–108.

Bleistein, N., 1987, On the imaging of reflectors in the earth: Geophysics, **52**, 931–942.

Bleistein, N., Y. Zhang, S. Xu, G. Zhang, and S. H. Gray, 2005, Migration/inversion: Think image point coordinates, process in acquisition surface coordinates: Inverse Problems, **21**, 1715–1744.

Brandsberg-Dahl, S., M. V. de Hoop, and B. Ursin, 2003, Focusing in dip and AVA compensation on scattering-angle/azimuth common image gathers: Geophysics, **68**, 232–254.

Ettrich, N., D. Merten, and S. K. Foss, 2008, True-amplitude angle migration in complex media: 70th Conference & Exhibition, EAGE, Extended Abstracts, 1632–1636.

Fomel, S., and J. A. Sethian, 2002, Fast-phase space computation of multiple arrivals: Proceedings of the National Academy of Sciences of the United States of America, **99**, 7329–7334.

Koren, Z., and I. Ravve, 2011, Full-azimuth subsurface angle domain wavefield decomposition and imaging: Part I — Directional and reflection image gathers: Geophysics, **76**, no. 1, S1–S13.

Koren, Z., S. Xu, and D. Kosloff, 2002, Target-oriented common reflection angle migration: 72nd Annual International Meeting, SEG, Expanded Abstracts, 1196–1199.

Miller, D., M. Oristaglio, and G. Beylkin, 1987, A new slant on seismic imaging: Migration and integral geometry: Geophysics, **52**, 943–964.

Operto, M. S., S. Xu, and G. Lambare, 2000, Can we quantitatively image complex structures with rays?: Geophysics, **65**, 1223–1238.

Sava, P. C., and S. Fomel, 2003, Angle-domain common-image gathers by wave field continuation methods: Geophysics, **68**, 1065–1074.

Schneider, W. A., 1978, Integral formulation for migration in two and three dimensions: Geophysics, **43**, 49–76.

Stolk, C. C., and W. W. Symes, 2004, Kinematic artifacts in prestack depth migration: Geophysics, **69**, 562–575.

Xu, S., H. Chauris, G. Lambare, and M. Noble, 2001, Common-angle migration: A strategy for imaging complex media: Geophysics, **66**, 1877–1894.

Xu, S., and G. Lambare, 2004, Fast migration/inversion with multivalued rayfields: Part 1 — Method, validation test, and application in 2D to Marmousi: Geophysics, **69**, 1311–1319.